



**HAL**  
open science

## Implantable CMOS pixel sensor for positron imaging in rat brain

J. Heymes, L. Ammour, M. Bautista, G. Bertolone, A. Dorokhov, S. Fieux, F. Gensolen, M. Goffe, C. Hu-Guo, M. Kachel, et al.

► **To cite this version:**

J. Heymes, L. Ammour, M. Bautista, G. Bertolone, A. Dorokhov, et al.. Implantable CMOS pixel sensor for positron imaging in rat brain. Nuclear Instruments and Methods in Physics Research Section A: Accelerators, Spectrometers, Detectors and Associated Equipment, 2018, 911, pp.19-24. 10.1016/j.nima.2018.09.117 . hal-01952201

**HAL Id: hal-01952201**

**<https://hal.science/hal-01952201>**

Submitted on 13 Mar 2019

**HAL** is a multi-disciplinary open access archive for the deposit and dissemination of scientific research documents, whether they are published or not. The documents may come from teaching and research institutions in France or abroad, or from public or private research centers.

L'archive ouverte pluridisciplinaire **HAL**, est destinée au dépôt et à la diffusion de documents scientifiques de niveau recherche, publiés ou non, émanant des établissements d'enseignement et de recherche français ou étrangers, des laboratoires publics ou privés.

# Implantable CMOS Pixel Sensor for Positron Imaging in Rat Brain

J. Heymes<sup>a,\*</sup>, L. Ammour<sup>b</sup>, M. Bautista<sup>d</sup>, G. Bertolone<sup>a</sup>, A. Dorokhov<sup>a</sup>, S. Fieux<sup>e</sup>, F. Gensolen<sup>d</sup>, M. Goffe<sup>a</sup>, C. Hu-Guo<sup>a</sup>, M. Kachel<sup>a</sup>, F. Lefebvre<sup>b</sup>, F. Pain<sup>b</sup>, P. Pangaud<sup>d</sup>, L. Pinot<sup>b</sup>, P. Gisquet<sup>f</sup>, P. Lanièce<sup>b</sup>, C. Morel<sup>d</sup>, M.-A. Verdier<sup>c</sup>, M. Winter<sup>a</sup>, L. Zimmer<sup>e</sup>, J. Baudot<sup>a</sup>

<sup>a</sup>Université de Strasbourg, CNRS, IPHC UMR 7178, F-67000 Strasbourg, France

<sup>b</sup>IMNC UMR 8165, Université Paris-Sud, Université Paris Diderot, CNRS/IN2P3, Université Paris Saclay, 91405 Orsay, France

<sup>c</sup>Univ. Paris-Diderot, Sorbonne Paris Cité, IMNC CNRS-IN2P3, 91405 Orsay, France

<sup>d</sup>Aix Marseille Université, CNRS/IN2P3, CPPM, Marseille, France

<sup>e</sup>CERMEP-Imagerie du vivant, Université Claude Bernard Lyon 1, CNRS, INSERM, Hospices Civils de Lyon, Lyon, France

<sup>f</sup>NeuroPSI CNRS/INSB, Univ Paris Sud, Orsay, France

## Abstract

IMIC is a Monolithic Active Pixel Sensor prototype designed for the MAPSSIC project, which aims at developing wireless intracerebral probes dedicated to image positron-emitting source activity in the brain of awake and freely moving rats. Former experiments with the PIXSIC positron probe based on a passive sensor have validated the proof of concept, but have also shown limitations with regards to the probe robustness and to its transparency to annihilation photons.

The IMIC circuit features a matrix of  $16 \times 128$  active pixels of  $30 \times 50 \mu\text{m}^2$  size and targets to overcome the PIXSIC probe drawbacks by exploiting a thin sensitive layer of  $18 \mu\text{m}$ , still featuring an overall thickness close to  $300 \mu\text{m}$ . Additionally, by using a low power ( $55 \text{ nW/pixel}$ ) in-pixel front-end architecture providing binary output, IMIC solves the challenge of implanting an active sensor in tissues where overheating is forbidden.

The needle-shaped sensor  $610 \mu\text{m} \times 12000 \mu\text{m}$  was fabricated and tested in laboratory. The whole sensor dissipates  $160 \mu\text{W}$  and its imaging capabilities were asserted with various sources :  $^{55}\text{Fe}$ ,  $^{90}\text{Sr}$  and  $^{18}\text{F}$ . These tests also demonstrated robust count-rate measurement with IMIC in the range  $10\text{--}1000$  counts/matrix/s. Finally, a dedicated setup qualitatively confirmed excellent in-sensitivity to  $511 \text{ keV } \gamma$ -rays.

In this paper, we present the sensor requirements and its detailed design. We also discuss the first characterisation results and the outlook for the integration of IMIC into an implantable probe.

**Keywords:** Semiconductor Detectors, CMOS Pixel Sensors, Beta Probe, Brain Imaging, Neuroimaging

## 1. Introduction

Neuroimaging results of anaesthetised or highly restrained animals suffers from undesired effects that are limiting their validity [1, 2]. In contrast, real time monitoring of molecular processes in brains of fully awake animals has a strong potential to improve the robustness of observations that couple neuroimaging and behavioural studies [3, 4]. Approaches based on PET imaging [5, 6, 7] have only partly achieved this goal due to a remaining mechanical support, or an overall weight, or a limited space that does not guarantee the animal freedom of movement for behavioral studies.

Another approach consists in performing invasive measurements using an autonomous positron sensitive probe implanted in specific brain regions by stereotaxic surgery. An advanced solution using a needle-shaped passive silicon sensor was developed with PIXSIC [8, 9, 10, 11]. Figure 1

illustrates the full PIXSIC concept. The miniaturisation of the sensor signal treatment within the PICPUS ASIC [9] allows wireless data transmission through a relative light system carried on a backpack. PIXSIC actually releases physical hindrances to the rodent movements. While invasiveness of this technique is a major point of concern, no impact from the small-size probe direct implantation was observed. However, the PIXSIC setup suffers from two main limitations.

First the length of the metallic lines that connect pixel sensors to their pre-amplification stages on the PICPUS readout chip induces EM pickup, which reduces signal over noise ratio and hence the overall probe sensitivity. The second weak point of PIXSIC pertains to the thickness of the passive sensor, which is constrained by antagonist requirements. On the one hand, mitigating the sensitivity to  $\gamma$ -rays generated by electron-positron annihilations, whose positions are not necessarily near the probe, requires a thickness as small as possible. On the other hand, a relatively thick sensor is beneficial to mechanical stiffness. A compromise of  $200 \mu\text{m}$  thickness was chosen for PIXSIC, though

\*. Corresponding author

Email address: julian.heyemes@iphc.cnrs.fr (J. Heymes)

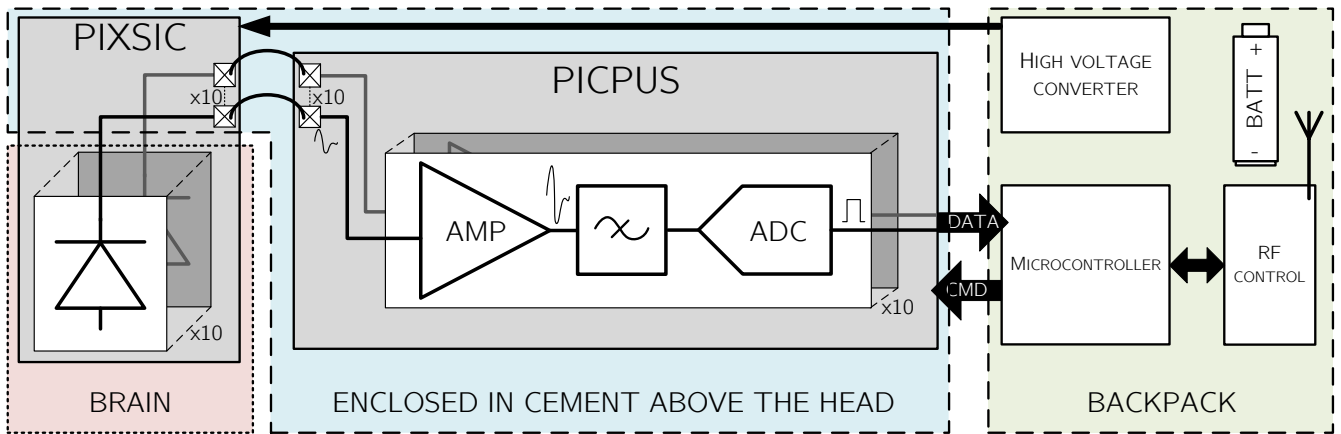


FIGURE 1: Schematic of the PIXSIC setup. The needle probe implanted in the brain is composed of 10 passive pixels, each directly wire-bonded to one channel of the readout chip : PICPUS. This chip embeds amplifiers, filter, digitisation, and memories, and is enclosed in dental cement above the skull. A micro-controller steers and gathers data from the readout chip. It is located on a backpack carried by the rodent during experiments. It also embeds active and passive circuits for the polarisation of the sensor and readout chip, and a battery for full autonomy.

41 it was not really satisfactory for both the constraints.

42  
 43 The usage of monolithic active pixels sensors (MAPS) 78  
 44 was proposed [12] to improve the implanted probe concept. 79  
 45 MAPS can embed an amplification and digitisation stage  
 46 in each pixel, basically replacing the PICPUS chip and  
 47 suppressing *a priori* sensitivity to electromagnetic envi- 80  
 48 ronment. Since the amplification allows a small primary 81  
 49 signal, the sensitive thickness can be thinner than the over- 82  
 50 all sensor thickness. Hence a depth of typically a few tens 83  
 51 of micrometers generate enough signal for efficient detec- 84  
 52 tion and does not need to extent to the full sensor thick- 85  
 53 ness also limiting its sensitivity to  $\gamma$ -rays. The latter can 86  
 54 be set optimally with respect to invasiveness and stiffness. 87  
 55 In addition, the probe integration is simplified due to the 88  
 56 absence of an additional circuit on the rodent head, as de- 89  
 57 picted in figure 2.

58  
 59 However, the usage of an implanted active sensor can 92  
 60 only be effective under the condition that the local tempe- 93  
 61 rature is marginally affected by the probe operation (typi- 94  
 62 cally  $\Delta T < 1^\circ\text{C}$ ). Consequently, a key design feature is the 95  
 63 power dissipated by the sensor.

64  
 65 Following the ideas developed in [12] along with the 98  
 66 requirement to minimize the power consumption, a first 99  
 67 MAPS based on the CMOS pixel sensors technology has 100  
 68 been developed. The chip is named IMIC (*Imageur Moléculaire*  
 69 *Intra-Cérébral*) and is part of the MAPSSIC (MAPS *Sonde*  
 70 *Intra-Crânienne*) project to develop and exploit the first 103  
 71 MAPS-based intracerebral positron probe.

72  
 73 This paper first describes in section 2 the requirements 106  
 74 for the active sensor to be implanted in the brain. The 107  
 75 design and operation features of IMIC, optimized for low 108

count rate and power dissipation, are detailed in section 3.  
 77 Section 4 provides first characterization results, focussing  
 on functional validation and sensitivity with laboratory  
 sources.

## 2. Sensor Requirements

Neuroimaging exploits a variety of radioactive isotopes,  
 typically  $^{18}\text{F}$ ,  $^{15}\text{O}$  and  $^{11}\text{O}$ , which emit  $\beta^+$  at energies  
 from 0 to 1.7 MeV. The probe ability to measure activi-  
 ties depends obviously on what energy range the sensor  
 is sensitive to. Consequently an important figure of merit  
 is the detection threshold, which should be as low as pos-  
 sible (this requirement is an outcome of the study in [12])  
 and depends on the signal-over-noise ratio of the sensing  
 element. The threshold value will be discussed in the next  
 section 3 in view of the sensitive thickness and noise level  
 of the designed sensors.

As previously mentioned, the usage of MAPS for this  
 kind of probe intends to both enhance the overall robust-  
 ness and simplify the system beyond the implanted part of  
 the probe. Thus, we have included into the requirements  
 the digital conversion of the signal inside the pixels hence  
 facilitating further data transmission. It is also expected  
 that the readout architecture of the sensor optimises data  
 throughput to the micro-controller embedded on the ani-  
 mal backpack with respect to the measured activity.

Regarding the sensors dimensions, we follow the ones of  
 the PIXSIC sensor (15 mm long, 500  $\mu\text{m}$  wide and 500  $\mu\text{m}$   
 thick), compatible with the requirements on invasiveness  
 [9].

Imaging the source and evaluating its activity require some  
 level of segmentation, especially along the (vertical) im-  
 plantation direction. The size of the pixels of the PIXSIC

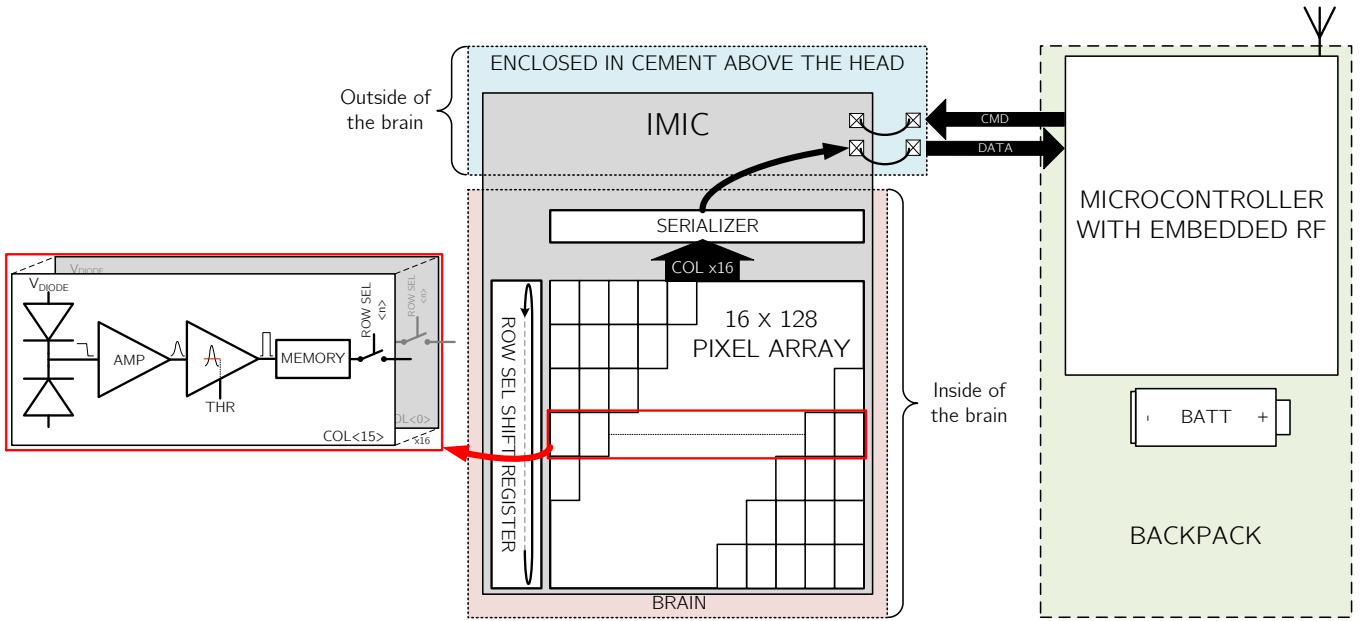


FIGURE 2: Schematic of the MAPSSIC setup. The monolithic active pixel sensor IMIC is a needle shaped probe composed of  $16 \times 128$  pixels of  $30 \times 50 \mu\text{m}^2$ , which provide binary information whether a pixel has been hit or not. IMIC is wire bonded to a PCB acting as an interface to the connector and is enclosed in cement on the head of the rodent. The chip is steered and read out only through digital signals by using a micro-controller located on the backpack together with a battery, which is embedding wireless transmission with the data acquisition PC.

109 probe were  $200 \times 500 \mu\text{m}^2$ , with no segmentations but<sup>139</sup>  
 110 along its length. Such a segmentation proved to be granu-<sup>140</sup>  
 111 lar enough to map subcortical brain activity [9] and there-<sup>141</sup>  
 112 fore should be matched quite easily by MAPS, which can<sup>142</sup>  
 113 feature much higher granularity.

114  
 115 According to first positron count rate observations with<sup>143</sup>  
 116 the PIXSIC probe [9], an average positron flux of about<sup>144</sup>  
 117 100 hits/sensor/s is expected over the required dimensions.<sup>145</sup>  
 118 This level of positron flux corresponds to at least three<sup>146</sup>  
 119 orders of magnitude less than standard achievements of<sup>147</sup>  
 120 CMOS pixel sensors used for charge particle detection.<sup>148</sup>  
 121 However, a stringent constraint arises from operation in<sup>149</sup>  
 122 a living animal brain.

123  
 124 As a matter of fact, active architectures involve power<sup>151</sup>  
 125 consumption and thus heat dissipation, which could locally<sup>152</sup>  
 126 overheat brain tissues in contact with the sensor. To avoid<sup>153</sup>  
 127 behavioural impact or worst, tissue damage, from excess<sup>154</sup>  
 128 heat dissipation, finite element computations were perfor-<sup>155</sup>  
 129 med in order to set a limit on the dissipated power. The sim-<sup>156</sup>  
 130 ulated geometry includes a volume of silicon representing<sup>157</sup>  
 131 the implanted part of the probe ( $10 \text{ mm} \times 500 \mu\text{m} \times 600 \mu\text{m}$ )<sup>158</sup>  
 132 in a spheric medium representing the brain at a constant<sup>159</sup>  
 133 temperature of  $37 \text{ }^\circ\text{C}$ . The highest temperature gradient<sup>160</sup>  
 134 at the direct probe contact stays below the required  $1 \text{ }^\circ\text{C}$ <sup>161</sup>  
 135 for a dissipated power below  $4 \text{ mW}$ . Considering the possi-<sup>162</sup>  
 136 ble implantation of multiple probes composed of 2 to 4<sup>163</sup>  
 137 sensors, we have set a limit of  $1 \text{ mW}$  dissipated per sensor.<sup>164</sup>  
 138 Due to the simplistic nature of the above calculation, the<sup>165</sup>  
 166

power of  $1 \text{ mW}$  per sensor is taken as an indicative limit.  
 The actual guideline chosen for the sensor design follows  
 the requirement to achieve the lowest possible power dis-  
 sipation.

### 3. IMIC sensor design

#### 3.1. Technology choice and overall geometry

We have chosen to design the sensor in the same im-  
 ager CMOS process with  $180 \text{ nm}$  feature size as used for  
 various charged particle detection applications [13]. The  
 sensitive volume consist of a  $18 \mu\text{m}$  thick low-doped epi-  
 taxial layer, which has demonstrated  $100 \%$  detection effi-  
 ciency for minimum ionising particles for various pixel  
 sizes below  $50 \mu\text{m}$  [13]. Such realization guarantee *a priori*  
 excellent detection performances for  $\beta^+$  within the energy  
 range of interest.

In addition, the thin detection layer presents two key ad-  
 vantages. First, it mitigates the sensitivity to the anni-  
 hilation photons as recommended in [12]. Secondly, it al-  
 lows thinning the sensor down to thicknesses from  $100$  to  
 $300 \mu\text{m}$ , thus achieving an optimum between invasiveness  
 and mechanical stiffness.

Regarding segmentation, we have opted for a rectan-  
 gular shape pixel, within the dimensions known to yield  
 excellent charge collection :  $30 \mu\text{m}$  wide and  $50 \mu\text{m}$  along  
 the vertical dimension of the probe. A matrix of  $16$  (ho-  
 rizontal)  $\times$   $128$  (vertical) pixels then covers a sensitive  
 area of  $480 \times 6400 \mu\text{m}^2$ , meeting the objective to create a

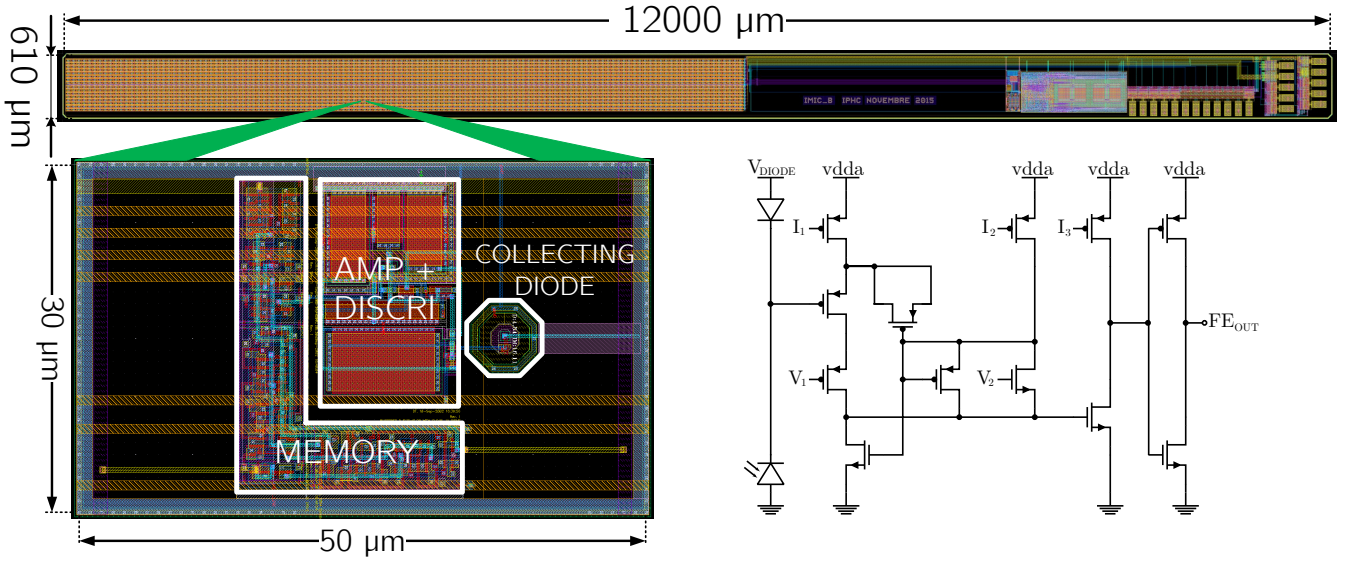


FIGURE 3: Top : layout of the 12000  $\mu\text{m}$  long and 610  $\mu\text{m}$  wide IMIC sensor. Bottom left : magnified layout of a single pixel underlying the location of its main functional components. Bottom right : Pixel circuit schematic derived from the ALPIDE sensor [14].

needle-shape probe.

The overall sensor dimensions reach 610  $\mu\text{m}$  width and 12 mm length. The vertical extension beyond the active matrix serves to implement the readout and control micro-circuits as well as the connection pads. The sensor is thinned by the foundry to 280  $\mu\text{m}$  and hence presents three different layers along its thickness : first 10  $\mu\text{m}$  of electronic process insensitive to particles, secondly 18  $\mu\text{m}$  of sensitive epitaxy and lastly roughly 250  $\mu\text{m}$  of silicon substrate that provides mechanical support.

The produced sensor layout is shown on the top of figure 3.

### 3.2. Pixel design

To satisfy simultaneously the main requirements on the pixel functionalities and performances (digital output, low data-throughput, low detection threshold and low power), a modified version of the ALPIDE (ALice PIlxel DETector) [14] circuit developed for the ALICE experiment is implemented. The initial compact pixel architecture amplifies, shapes (with clipping to prevent saturation), and discriminates the signal collected by the diode using only 12 transistors, as depicted on the bottom of figure 3). Pixels integrate any incoming charge between two consecutive readouts. Since the binary output of the front-end indicating the presence of a hit is only available for a few tens of  $\mu\text{s}$ , a 1-bit memory was added per pixel to keep this information until the pixel readout time. The memory is reset after the pixel is read out, so that if a second particle hit the same pixel before readout, the 1-bit memory cannot account for it. The matrix readout strategy is detailed

in the next sub-section.

Simulations of the pixel architecture using Cadence Virtuoso Analog Design Environment have evaluated the equivalent noise charge (ENC) at the collection node below 10 electrons, hence allowing to set discriminators for the digitisation at an equivalent level of  $\approx 100 e^-$ . The corresponding energy threshold for the detection equals  $\approx 360 \text{ eV}$ , well below the maximum probability value of energy loss in 18  $\mu\text{m}$  of silicon by  $\beta^+$  with energies within 0 to 2 MeV.

Finally, these simulations predict that the overall front-end dissipates about 55 nW per pixel (or 113  $\mu\text{W}$  for the whole matrix), well below the upper limit. The schematic of the pixel and its layout are shown in figure 3.

### 3.3. Readout strategy

IMIC readout mechanism is kept simple for the sake of space and power dissipation, which does not depend on the hit rate, and relies on the rolling-shutter principle. A token is propagated through the matrix in a shift register at a fixed clock rate to select one line. The 16-bits word formed by all the pixel memories in the line is serialised towards the output of the sensor at a higher clock rate (at least 16 times), which defines  $f_{\text{clock}}$ . This operation is repeated 128 times to gather data from the entire pixel array, thus the time  $t_{\text{readout}}$  needed for this full readout cycle amounts to

$$t_{\text{readout}} = \frac{2048}{f_{\text{clock}}} \quad [\text{s}]. \quad (1)$$

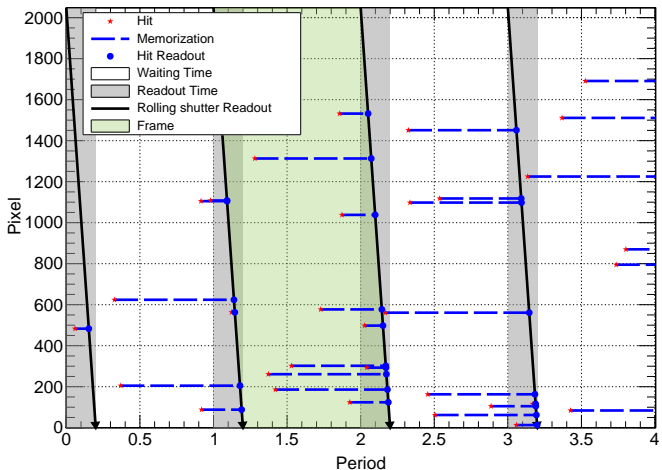


FIGURE 4: Readout strategy for IMIC. When a pixel detects a hit, the event is memorised until rolling-shutter readout. A frame is composed of an adjustable waiting time and the readout time. During the readout, the data of each pixel is sent outside the sensor, bit after bit. The data of the memory is reset after readout to allow the detection and memorisation of a new hit.

229 Pixels integrate particle hits during the time  $t_{wait}$  between  
230 two readout cycles, plus the readout time itself :

$$231 \quad t_{integration} = t_{readout} + t_{wait} \quad [s]. \quad (2)$$

232 For each readout cycle, data are provided to the micro-  
233 controller as a vector of 2048 bits to be sent further away  
234 through a wireless protocol. In view of limiting the data  
235 rate defined by equation 3 and hence the overall power  
236 consumption of the MAPSSIC setup, it is better to maxi-  
237 mize the waiting time  $t_{wait}$  during two readout cycles. Ho-  
238 wever, avoiding pile-up of hits during the same integration  
239 period requires to minimise  $t_{wait}$ .

$$241 \quad Data\ rate = \frac{2048}{t_{integration}} \quad [bits/s] \quad (3)$$

242 The foreseen average hit-rate of about 100 hits/matrix/s  
243 in our experiments, leads to an optimisation for the inte-  
244 gration time of around 50 millisecond. In such conditions  
245 the data rate stays at a few tens of kilo-bits per second  
246 while keeping the pile-up probability at the per mil level.  
247 Figure 4 depicts the principle of operation of the IMIC  
248 readout.

### 249 3.4. A fully programmable needle shaped sensor

250 In order to minimize the complexity of the external cir-  
251 cuitry, IMIC limits the number of required connections by  
252 using a command decoder controlled through Serial Per-  
253 ipheral Interface (SPI) protocol. This controller also allows  
254 the parametrisation of on-chip digital-to-analog converters  
255 (DACs) used for the polarisation of the front-end. The  
256 steering signals (and the data) are sent independently bet-  
257 ween the micro-controller located on the rodent backpack

258 and the sensor. The micro-controller connects to the exter-  
259 nal world through a wireless protocol. The overall system  
260 description will be the subject of a subsequent publica-  
261 tion.

262 The digital block driving IMIC is located on the sensor  
263 edge near the few connection pads located outside of the  
264 brain, opposite to the pixel matrix deeply implanted in the  
265 tissues. This block adds a power consumption of approxi-  
266 mately 2  $\mu$ W. The simulated total IMIC power consump-  
267 tion amounts to approximately 115  $\mu$ W. This dissipation  
268 does not depend on the activity measured but is entirely  
269 driven by the number of pixels populating the matrix.

The main characteristics of the IMIC sensor are sum-  
271 marised in table 1.  
272

TABLE 1: Summary of the simulated characteristics of the IMIC sen-  
sor.

Feature	Value
Sensor size [ $\mu\text{m}^3$ ]	$610 \times 12000 \times 280$
Pixel pitch [ $\mu\text{m}^2$ ]	$30 \times 50$
Sensitive depth [ $\mu\text{m}$ ]	18
Det. threshold [eV deposited]	$\approx 400$
Pixel power consumption [nW/pixel]	$\approx 55$
Matrix size	$16 \times 128$
Sensitive area [ $\mu\text{m}^2$ ]	$480 \times 6400$
Total power consumption [ $\mu\text{W}$ ]	$\approx 115$

## 4. IMIC characterisation

### 4.1. First images

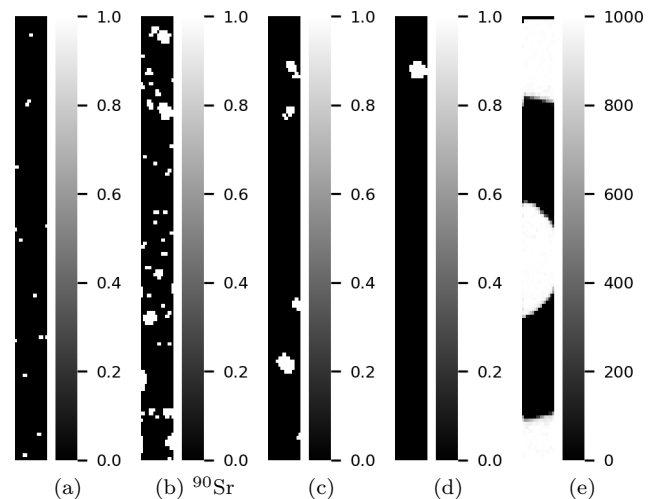


FIGURE 5: Images acquired with the IMIC sensor. Single frame ac-  
quired with a  $^{55}\text{Fe}$  soft-X-ray source (5a), a  $^{90}\text{Sr}$   $\beta$  source (5b), and  
a  $^{18}\text{F}$  positron source (5c). A single annihilation photon from the  
 $^{18}\text{F}$  positron source hit (5d). Image composed of 1000 accumulated  
frames of a metallic spacer acquired with  $^{55}\text{Fe}$  (5e).

A few IMIC sensors were bonded to a printed circuit  
board (PCB) in order to facilitate the first tests. After ad-  
justment of the various polarisations through the on-chip

DACs driven by the SPI protocol, the bonded chips were confirmed to be fully functional. All results reported below were obtained with these sensors at room temperature under relative obscurity.

The measured dissipated power by the whole sensor is 160  $\mu$ W, close to the value expected from simulations in table 1 considering the low absolute value for a complete chip.

Three types of sources have been used to characterise the IMIC sensor. Single frames from each source type are displayed in figures 5a–5d. Soft X-rays (5.9 and 6.4 keV rays) from the  $^{55}\text{Fe}$  source (figure 5a) generate small clusters of mainly two pixels, while the  $\beta$  particles, either from  $\beta^-$  ( $^{90}\text{Sr}$  : figure 5b) or from  $\beta^+$  ( $^{18}\text{F}$  : figure 5c) yield clusters about ten times larger in average. This difference comes from the relatively long ionising path of  $\beta$ -rays in silicon. In contrast, X-rays undergo point-like conversion through photoelectric effect.

Images from 511 keV  $\gamma$ -rays were obtained by placing the  $^{18}\text{F}$  source far away (see sub-section 4.3) from the sensor. The cluster size observed for these  $\gamma$ -rays is similar to the one for positrons (see figure 5d). This indicates that the cluster size information cannot be used to identify (and suppress) the unwanted  $\gamma$ -rays hits on an individual basis information.

To demonstrate that the sensor internal readout performs as expected, an image of a metallic washer was acquired using the  $^{55}\text{Fe}$  source (as shown in figure 5e). The ring is approximately 500  $\mu\text{m}$  thick with an external diameter of 5 mm and an opening diameter of 2 mm. The ring structure can easily be recognized on the image as it completely stops the soft X-rays.

#### 4.2. Validation of long integration times

As explained in section 3, the modest awaited activities of the radiotracers allow running the IMIC sensor with a long integration time in the order of 100 ms, which in turn reduces the data flow and simplifies the whole system. This readout strategy is made possible by the in-pixel memory and was tested by measuring a range of activities at integration times varying from 20 ms to 1 s.

For this test, the IMIC sensor was indirectly illuminated with a  $^{90}\text{Sr}$   $\beta$  source through an aluminium shield. The activity was modulated using three different aluminium thicknesses : 1, 3 and 7 mm. Additional measurements were performed without the source in order to monitor dark count rate. For each combinations of shield and integration time, 1000 frames were acquired with the same detection threshold. Results are presented in figure 6. The mean entries per integration time were converted into a mean activity measured over the whole matrix :

$$\overline{\mathcal{A}(t_{int})} = \frac{\text{entries}}{t_{int}} \quad [\text{hits/matrix/s}]. \quad (4)$$

The saturation limit corresponds to the situation where every pixel over the matrix has been fired. This limit depends on the integration time through the simple relation :

$$\mathcal{A}_{sat}(t_{int}) = \frac{2048}{t_{int}} \quad [\text{hits/matrix/s}]. \quad (5)$$

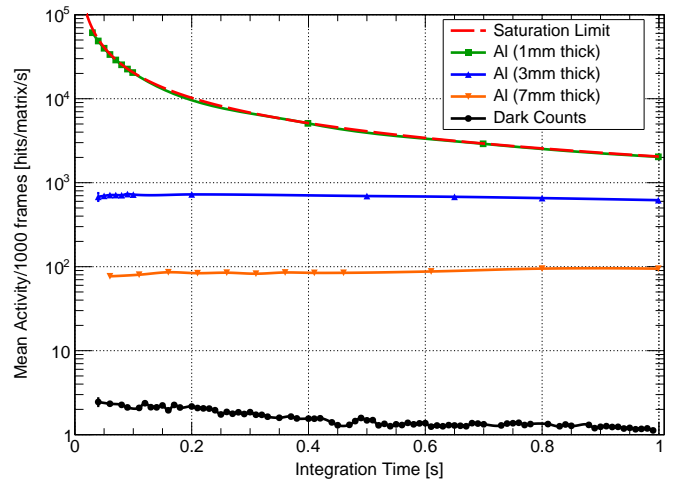


FIGURE 6: Mean activity seen by the sensor for integration times between 20 ms and 1 s of the IMIC sensor dark counts, and with various activities of  $^{90}\text{Sr}$   $\beta$ -rays modulated by using various aluminum shielding thicknesses.

The analysis of the dark count map revealed that a few pixels (denominated noisy pixels in the following) dominate the production of fake hits, which explains the dark count rate evolution with the integration time. As there are one to two noisy pixels systematically firing during one integration period, it follows that the dark count rate simply decreases as  $1/t_{integration}$  along with equation 4. The low level for the dark count rate means that the IMIC sensor can measure robustly activities down to approximately 10 hits/matrix /s.

With the  $^{90}\text{Sr}$  source attenuated by only 1 mm of aluminium, the mean activity follows the saturation limit curve. At  $t_{int} = 10$  ms, the mean activity seen by the sensor is approximately 60000 hits /matrix/s.

Using thicker shielding, the mean activity on the sensor remains below the saturation limit and is constant for every integration time. Thus, in the ballpark of expected average activities (100 hits/matrix/s), integration time up to 1 s can be chosen without information loss and with a safety margin against activity fluctuation of one order of magnitude. This read-out condition allows low data rates, and limits the power consumption of the overall system.

#### 4.3. Preliminary sensitivity study

Measurements using  $^{18}\text{F}$  radioisotope, produced at the CYRCé cyclotron at IPHC, in a non-sealed aqueous solution were performed in view of studying the differential sensitivity to prompt  $\beta^+$  and annihilation photons.

A first 3D printed tank contained a diluted solution of  $^{18}\text{F}$

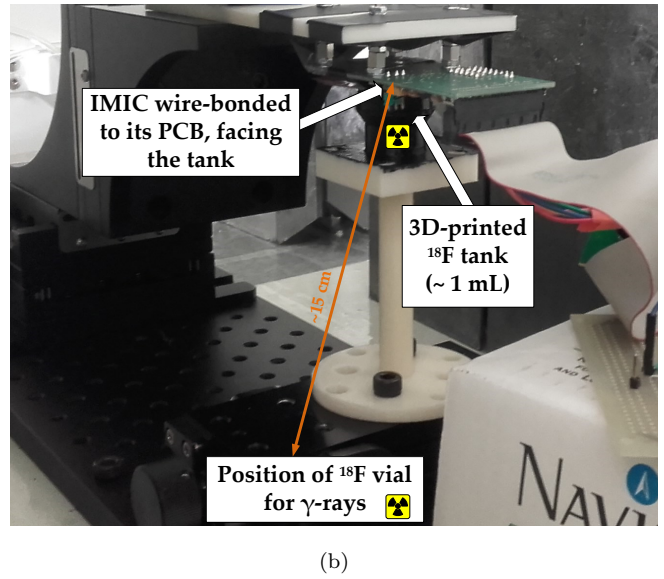
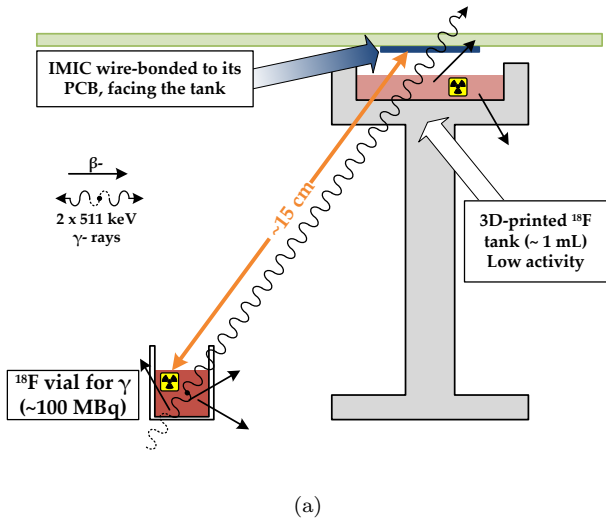


FIGURE 7: Experimental setup dedicated to measurements with  $^{18}\text{F}$ . The IMIC sensor wire-bonded to its PCB is closely oriented towards a first tank containing an aqueous solution of  $^{18}\text{F}$ . A vial of the same radiotracers with an higher activity was put on demand 15 cm away from the sensor in order to mimic the presence of a parasitic  $\gamma$ -ray source.

365 presenting an activity of about 1 MBq. The tank was de-376  
 366 signed to precisely position the sensor bonded to its PCB377  
 367 5 mm away from the solution. Since the source was dissol-378  
 368 ved in saline solution, the sensor was protected by plastic379  
 369 wrap. 380  
 370 Another vial filled with the same isotope but featuring a381  
 371 much higher activity of 100 MBq was disposed on demand382  
 372 15 cm away from the sensor. This second tank served as a383  
 373 parasitic source of 511 keV  $\gamma$ -rays, since the air distance384  
 374 and the glass of the vial (the opening needed to fill the385  
 375 vial is not oriented towards the sensor), fully attenuates386

positrons. This setup presented in figure 7 intends to re-  
 produce roughly the head-bladder relative positions in a  
 rat.

Data were taken with the IMIC sensor in three configura-  
 tions, for 5 minutes each. The observed counts per time  
 and average count rate are plotted in figure 8a, where the  
 average count rates are corrected for the time decay of  $^{18}\text{F}$ .  
 Count distributions observed with both tanks present are  
 labeled  $^{18}\text{F}+\gamma$ , the distributions obtained with only the  
 tank close to the sensor is tagged  $^{18}\text{F}$ , and finally the label

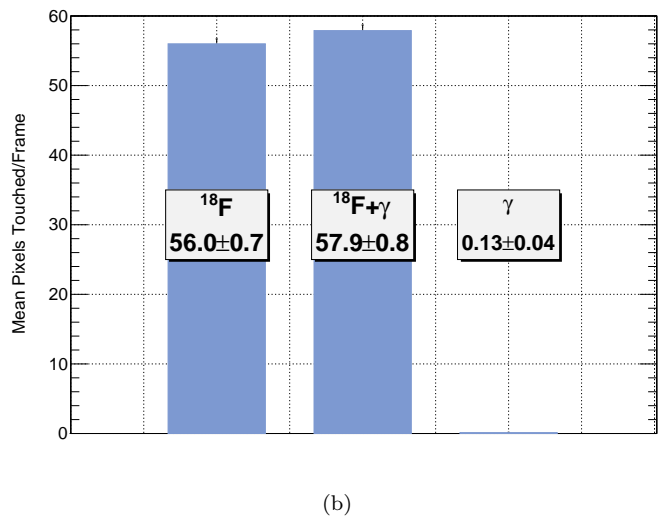
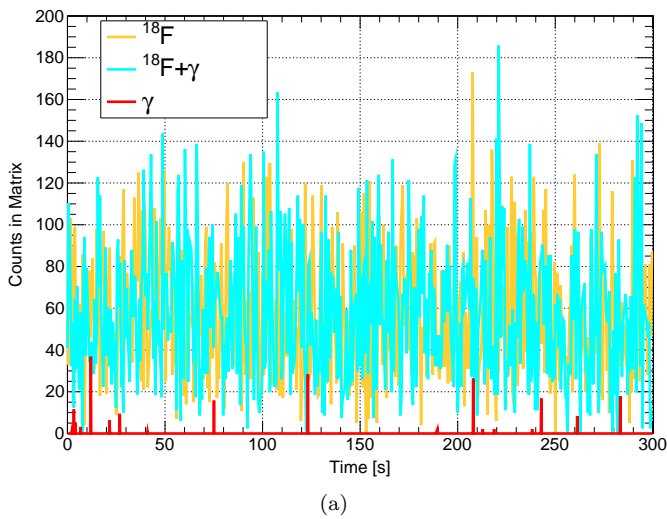


FIGURE 8: Left : Evolution with time of the pixel count per 100 ms frame duration for the three source configurations described in the text. Right : Average pixel count per frame over five minutes data acquisition for the same configurations.

is  $\gamma$  when only the distant tank was used.

The counting rates for the three source configurations are displayed in figure 8b. Within uncertainties, the average counting rate with both sources ( $^{18}\text{F}+\gamma$ ) or only with the closer tank ( $^{18}\text{F}$ ) are equivalent, they amount respectively to  $56.0 \pm 0.7$  and  $57.9 \pm 0.8$  pixels/frame. This observation is coherent with the very small counting rate ( $0.13 \pm 0.04$  pixels/frame) measured when only the far-away source ( $\gamma$ ) is used.

The experiment illustrates qualitatively the very small relative sensitivity of the thin IMIC sensor to  $\gamma$ -rays with respect to  $\beta+$ .

## 5. Conclusion

Following [12], we have designed a monolithic active pixel sensor to equip the next generation of intracerebral positron probes for deep brain imaging adapted to fully conscious and freely moving rodents. The IMIC chip features 2048 active pixels over a sensitive area of  $480 \times 6400 \mu\text{m}^2$ . The in-pixel amplification and 1-hit binary memory allows both a low detection threshold (400 eV for the energy deposited) and fully digital matrix readout. This front-end architecture benefits from an extremely low power, addressing the main challenge of heat dissipation within the implantation tissues. Finally, being fabricated on a  $18 \mu\text{m}$  thick sensitive layer, the sensor is mostly transparent to  $\gamma$ -rays.

The first IMIC sample characterisations confirmed the successful operation of the sensor as a  $\beta+$  activity locator. The measured power dissipation per sensor reached  $160 \mu\text{W}$ . This performance sets the current state-of-the-art for a probe built on the CMOS pixel technology, and should allow the implantation of a few probes in a single animal with acceptable overheating of the local brain tissues. Foreseen *in-vivo* experiments will be conducted to investigate the full compliance of the IMIC sensor with the application requirements.

A second generation sensor can benefit from a fully depleted thin sensitive layer, which would allow to increase the pixel size, hence decrease the total number of pixels and leading to a reduction of the total dissipated power.

Currently, pairs of IMIC sensors are assembled back-to-back to form the implantable part of the final MAPSSIC probe with a total volume of  $560 \times 610 \times 12000 \mu\text{m}^3$ . The rest of the construction process for the whole probe and its tests in realistic environment will be the subject of a forthcoming publication.

## Acknowledgement

This work was partly funded in 2015 and 2017 by the project *Instrumentation aux limites* from CNRS.

This work was partly funded by France Life Imaging,

FLI/ANR-11-INBS-0006, of the French *Investissements d'Avenir* program run by the *Agence Nationale pour la Recherche*.

This work was partly funded by the IN2P3.

The authors thank the CYRCé team at IPHC for producing and making available the  $^{18}\text{F}$  solutions.

## References

- [1] Y.-R. Gao, Y. Ma, Q. Zhang, A. T. Winder, Z. Liang, L. Antinori, P. J. Drew, N. Zhang, Time to wake up : Studying neurovascular coupling and brain-wide circuit function in the unanesthetized animal, *NeuroImage* 153 (Supplement C) (2017) 382 – 398.
- [2] A. K. O. Alstrup, D. F. Smith, Anaesthesia for positron emission tomography scanning of animal brains, *Laboratory Animals* 47 (1) (2013) 12–18.
- [3] C. Carter, *Brain Imaging in Behavioral Neuroscience*, Vol. 11, Springer-Verlag Berlin Heidelberg, 2012.
- [4] S. Chery, Functional whole-brain imaging in behaving rodents, *Nature Methods* 8 (4) (2011) 301–303.
- [5] V. D. Patel, D. E. Lee, D. L. Alexoff, S. L. Dewey, W. K. Schiffer, Imaging dopamine release with Positron Emission Tomography (PET) and 11C-raclopride in freely moving animals, *NeuroImage* 41 (3) (2008) 1051 – 1066.
- [6] A. Z. Kyme, V. W. Zhou, S. R. Meikle, C. Baldock, R. R. Fulton, Optimised Motion Tracking for Positron Emission Tomography Studies of Brain Function in Awake Rats, *PLOS ONE* 6 (7) (2011) 1–16.
- [7] D. Schulz, Integrating PET with behavioral neuroscience using RatCAP tomography, *Reviews in the Neurosciences* 22 (6) (2011) 647–655.
- [8] J. Märk, D. Benoit, L. Balasse, M. Benoit, J. C. Clémens, S. Fieux, D. Fougere, J. Graber-Bolis, B. Janvier, M. Jevaud, A. Genoux, P. Gisquet-Verrier, M. Menouni, F. Pain, L. Pinot, C. Tourviale, L. Zimmer, C. Morel, P. Laniece, A wireless beta-microprobe based on pixelated silicon for in vivo brain studies in freely moving rats, *Physics in Medicine & Biology* 58 (13) (2013) 4483.
- [9] J. Godart, P. Weiss, B. Chantepie, J. C. Clemens, P. Delpierre, B. Dinkespiler, B. Janvier, M. Jevaud, S. Karkar, F. Lefebvre, R. Mastroiolo, M. Menouni, F. Pain, P. Pangaud, L. Pinot, C. Morel, P. Laniece, PIXSIC : A Pixelated Beta-Microprobe for Kinetic Measurements of Radiotracers on Awake and Freely Moving Small Animals, *IEEE Transactions on Nuclear Science* 57 (3) (2010) 998–1007.
- [10] L. Balasse, J. Maerk, F. Pain, A. Genoux, S. Fieux, C. Morel, P. Gisquet-Verrier, L. Zimmer, P. Laniece, PIXSIC, a Pixelated  $\beta+$ -Sensitive Probe for Radiopharmacological Investigations in Rat Brain : Binding Studies with [ $^{18}\text{F}$ ]MPPF, *Molecular Imaging and Biology* 17 (2) (2015) 163–167.
- [11] L. Balasse, J. Maerk, F. Pain, A. Genoux, S. Fieux, F. Lefebvre, C. Morel, P. Gisquet-Verrier, P. Laniece, L. Zimmer, PIXSIC : A Wireless Intracerebral Radiosensitive Probe in Freely Moving Rats, *Molecular Imaging* 14 (9).
- [12] Ammour, et al., MAPSSIC, a Novel CMOS Intra-Cerebral  $\beta+$  Probe for Deep Brain Imaging in Awake and Freely-Moving Rat : a Monte-Carlo Study, Submitted to *IEEE Transactions on Radiation and Plasma Medical Sciences*.
- [13] J. Baudot, A. Besson, G. Claus, W. Dulinski, A. Dorokhov, M. Goffe, C. Hu-Guo, L. Molnar, X. Sanchez-Castro, S. Senyukov, M. Winter, Optimisation of CMOS pixel sensors for high performance vertexing and tracking, *Nuclear Instruments and Methods in Physics Research Section A : Accelerators, Spectrometers, Detectors and Associated Equipment* 732 (2013) 480 – 483.
- [14] M. Mager, ALPIDE, the Monolithic Active Pixel Sensor for the ALICE ITS upgrade, *Nuclear Instruments and Methods in Physics Research Section A : Accelerators, Spectrometers, Detectors*

506 and Associated Equipment 824 (Supplement C) (2016) 434 –  
507 438.